Applied Physics Letters

High frequency lithium niobate film-thickness-mode optomechanical resonator

Cite as: Appl. Phys. Lett. **117**, 131104 (2020); https://doi.org/10.1063/5.0020019
Submitted: 28 June 2020 . Accepted: 18 September 2020 . Published Online: 29 September 2020

Mohan Shen, Jiacheng Xie, Chang-Ling Zou, Yuntao Xu, Wei Fu, and Hong X. Tang

Applied Physics Letters ARTICLE scitation.org/journal/apl

High frequency lithium niobate film-thickness-mode optomechanical resonator

Cite as: Appl. Phys. Lett. **117**, 131104 (2020); doi: 10.1063/5.0020019
Submitted: 28 June 2020 · Accepted: 18 September 2020 ·
Published Online: 29 September 2020

Mohan Shen,[1] Jiacheng Xie,[1] Chang-Ling Zou,[2] Yuntao Xu,[1] Wei Fu,[1] and Hong X. Tang[1,a)]

AFFILIATIONS

[1]Department of Electrical Engineering, Yale University, New Haven, Connecticut 06511, USA
[2]Key Laboratory of Quantum Information, Chinese Academy of Sciences, University of Science and Technology of China, Hefei, 230026 Anhui, People's Republic of China

[a)]Author to whom correspondence should be addressed: hong.tang@yale.edu

ABSTRACT

High-frequency optomechanical resonators are in demand as transduction devices to bridge microwave and optical fields. Thin-film lithium niobate is a promising platform for implementing high-frequency optomechanics for its low optical loss and strong piezoelectric coefficients. However, its strong piezoelectricity is also known to introduce excess phonon loss. Here, we present lithium niobate optomechanical resonators with film-thickness-mode mechanical resonances up to 5.2 GHz, reaching the operating frequency regime of superconducting qubits. By engineering the mechanical anchor to minimize the phonon loss, we achieve a high quality factor up to 12 500 at cryogenic temperatures and, hence, a frequency-quality factor product of 6.6×10^{13}. Our system also features interference between piezo-optomechanical and electro-optic modulation. A theoretical model is derived to analyze these two effects and their interference.

Phonons piezoelectrically coupled to microwaves have enabled active control and manipulation of light[1–5] and coherent signal conversion between microwave and optical domains.[6–10] To effectively couple microwaves and phonons, significant effort has been focused on piezoelectric materials such as aluminum nitride,[11,12] gallium nitride,[13] and gallium arsenide[14,15] in a variety of device structures. However, to realize both high optical and mechanical quality factors, strong electromechanical and optomechanical coupling (MO) on a single platform is still challenging. The thin-film lithium niobate-on-insulator (LNOI) platform with large electro-optic (EO), acousto-optic, and piezoelectric coefficients[16] has recently drawn tremendous attention. High quality factor optical[17,18] and mechanical resonators[19] and efficient microwave-to-mechanical coupling efficiency[18] have been demonstrated on the LNOI platform recently. On the other hand, pushing for higher frequency mechanical mode is also of great importance such as in quantum optomechanics in order to reduce thermal occupation. Another critical parameter for optomechanical systems is the mechanical frequency-quality factor (fQ) product, which plays an important role in demonstrating quantum optomechanics and entanglement creation at elevated bath temperatures.[20–22] Therefore, in optomechanics experiments, it is essential to achieve high mechanical modal frequency f and fQ products simultaneously.

Piezoelectricity enables efficient coupling of microwave to phonon modes. However, the same coupling is also responsible for excess piezoelectric losses.[23,24] Previously, we have shown that AlN-based piezo-optomechanical resonators can operate at the microwave X-band[25] and its use for microwave-to-optics coherent conversions.[9] $LiNbO_3$, being a stronger piezoelectric material than AlN, promises to deliver even higher microwave-to-optics coupling efficiency if similar mechanical performance can be realized. Recently, high fQ product (on the order of $10^{12} - 10^{13}$) MEMS resonators based on $LiNbO_3$ thin films have been reported.[26,27] Here, in this paper, we demonstrate piezo-optomechanical racetrack resonators on thin film lithium niobate with mechanical resonance as high as 5.2 GHz, realized by exploiting the film thickness mode of suspended waveguides. The mechanical modes are driven by two electrodes placed across a gap from the suspended waveguide and readout optomechanically. By engineering the mechanical anchors, we achieve a high quality factor of 12 500 at 4 K, leading to an fQ product of 6.6×10^{13}, a value approaching that of the state-of-the-art cryogenic AlN devices.[9] The mechanical anchor design also preserves the high optical quality factor of around 2×10^6, allowing operations in the resolved-sideband regime. Due to the coexistence of the acousto-optic and electro-optic effect in lithium niobate, our system exhibits interference between opto-mechanical and electro-optic modulation for which we present a detailed analysis for effective extraction of the mechanical quality factor.

On the LNOI platform, partially etched waveguide resonators show the highest optical quality factor compared to photonic crystal

and microdisk resonators.[17] The cross section of this type of waveguide normally has a width of a few micrometers and a thickness of several hundreds of nanometers. With the thickness being the smaller dimension, thickness mode-like mechanical modes will possess higher frequency with its wavevector along the thickness direction.[25] On the other hand, to drive mechanical modes using on-chip electrodes, coplanar electrodes can be more easily realized from the fabrication point of view, which will produce electric fields mainly in the in-plane direction. Given the vanishing d_{31} and d_{32} piezoelectric tensor elements of lithium niobate,[16] X-cut LNOI would allow us to excite thickness mode-like mechanical modes using the in-plane electric field, while this cannot be done with Z-cut LNOI. Therefore, our devices are fabricated on a commercial X-cut LNOI wafer with a 600 nm-thick lithium niobate film.

Figure 1(a) shows a fully suspended racetrack resonator. In the fabrication process, the lithium niobate film is etched twice using Argon milling with patterned hydrogen silsesquioxane (HSQ) as resist. The lithium niobate film is first etched by 350 nm to fabricate half-etched optical waveguides. The second etch stops at the silicon dioxide layer and defines the slab. The slab under the optical waveguide is 3.5 μm wide and is connected with large slab pads through narrow links as shown in Figs. 1(b) and 1(c). These links provide support for the optical waveguide after being released. The narrow links also unavoidably introduce anchor loss for the mechanical modes, and so

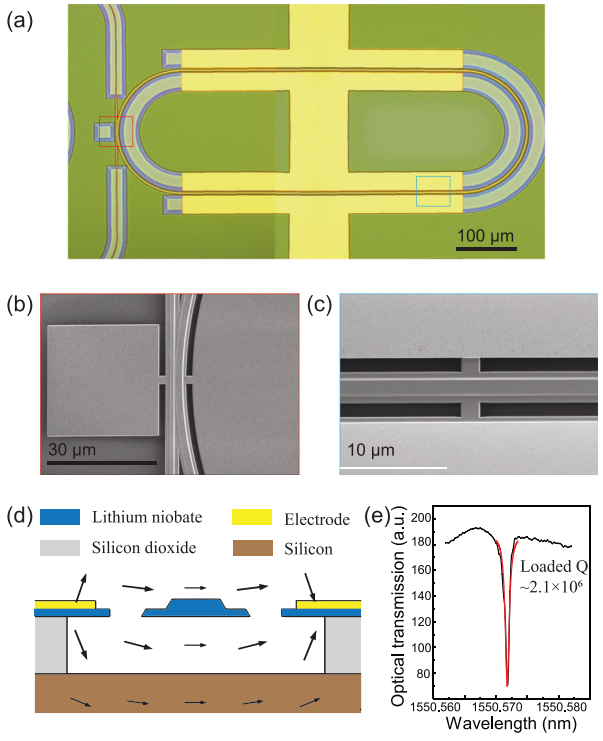

FIG. 1. (a) Optical image of a racetrack piezo-optomechanical resonator. The yellow part is deposited gold electrodes. (b) SEM image of the coupling part of the racetrack resonator. (c) SEM image showing the suspended optical waveguide supported by the slab. (d) Cross section of the released optomechanical waveguide structure and simulated electric field (shown by arrows) (e) Optical transmission spectrum of the resonator showing a loaded quality factor of 2.1×10^6.

the spacing between the anchors along the optical waveguide should be not only as long as possible to reduce anchor loss but also not too far apart; otherwise, the optical waveguide may break without sufficient support. In our devices, this spacing is chosen to be 50 μm.

After etching lithium niobate, 300 nm thick gold electrodes are deposited through liftoff using polymethyl methacrylate (PMMA) resist. Electrodes are placed along the arms of the racetrack resonator at both sides. The electrode-to-electrode gap is 8.1 μm. This narrow gap can provide a strong electric field but still large enough to prevent metal-induced photon absorption. Finally, the optical racetrack is fully released by removing the underneath 2 μm-thick silicon dioxide in buffered oxide etchant (BOE), while the slabs across the air gap from the released waveguide still have silicon dioxide underneath and provide side-anchors for mechanical suspension. In this design, the optical mode is well confined in the half-etched waveguide, does not see the discontinuity along the edges of the slab, and, therefore, prevents scattering loss and maintains the high quality factor of the optical resonator. Figure 1(e) shows an optical TE mode resonance around 1550 nm of a racetrack resonator fabricated from this fabrication process, which has a fitted quality factor of 2.1×10^6.

By applying a RF drive on the electrodes, a horizontal electric field is formed, which excites the mechanical motion of the suspended arm and, thus, in turn, modulates light in an optical cavity, via moving the boundary effect[28] as well as the elasto-optic effect. We denote this optical modulation induced by electrically excited mechanical motion electrical–mechanical–optical (EMO) modulation. Besides, the applied electric field also directly modulates the optical field through the electro-optic (EO) effect. To characterize the modulation efficiency through the two different mechanisms, we define two parameters as follows:

$$g_{EO} = -\frac{\partial \omega}{\partial V_0}\Big|_{EO}, \tag{1}$$

$$g_{EMO} = -\frac{\partial \omega}{\partial V_0}\Big|_{EMO}, \tag{2}$$

where ω is the optical resonance frequency and V_0 is the voltage amplitude applied between the electrodes. These two parameters measure the modulation efficiency by the optical resonance frequency shift under a unit microwave voltage drive.

For the electro-optic interaction,

$$g_{EO} = -\frac{\partial \omega}{\partial V_0}\Big|_{EO} = \frac{\omega_0}{2}\frac{\int \sum_{ij} E_i \cdot (d\varepsilon_{ij}/dV_0) \cdot E_j dV}{\int \vec{E} \cdot \vec{D} dV}, \tag{3}$$

with $d\varepsilon_{ij}/dV_0 = -\sum_k \varepsilon_{ij}^2 r_{ijk} E_k^{mw}$, where E^{mw} is the microwave electric field when the voltage between the electrodes is 1 V and r_{ijk} is the third rank electro-optic tensor. Compared to the EO effect, EMO modulation features a strong frequency dependence due to mechanical resonance. This dependence can be separated into two cascaded parts, the microwave to mechanical coupling and optomechanical coupling, or $g_{EMO} = -\frac{\partial \omega}{\partial V_0}|_{EMO} = -\frac{\partial \omega}{\partial \alpha}\frac{\partial \alpha}{\partial V_0}$, where α is the maximum mechanical displacement within the waveguide. The response of a driven harmonic oscillator gives $\alpha = g_{EM} V_0 / \sqrt{(\Omega^2 - \Omega_b^2)^2 + \Gamma_m^2 \Omega^2}$, $\varphi_m = \arctan(-\Gamma_m \Omega / (\Omega_b^2 - \Omega^2))$, where g_{EM} is a constant, Ω_b is the

mechanical resonant angular frequency, Γ_m is the mechanical mode loss rate, and Ω is the driven frequency. The optomechanical coupling (MO) can be described by[1]

$$g_{MO} = -\frac{\partial\omega}{\partial\alpha} = \frac{\omega_0}{2}\frac{\int\left(\Delta\varepsilon\vec{E_\tau}^{\,2} - \Delta\frac{1}{\varepsilon}\vec{D_n}^{\,2}\right)(\vec{q}(\vec{r})\cdot\hat{n})dS + \int\sum_{ij} E_i\frac{d\varepsilon_{ij}}{d\alpha}E_j dV}{\int\vec{E}\cdot\vec{D}dV}, \tag{4}$$

with $d\varepsilon_{ij}/d\alpha = -\varepsilon_{ij}^2(\sum_{kl} p_{ijkl}u_{kl} + \sum_k r_{ijk}E_{pk})$, where ω_0 is the optical resonant frequency, $\vec{q}(\vec{r})$ is the normalized mechanical displacement field, $\vec{E_\tau}$ is the tangential electric field at the boundary, $\vec{D_n}$ is the normal electric displacement field at the boundary, p_{ijkl} is the fourth rank elasto-optic tensor, r_{ijk} is the third rank electro-optic tensor, u_{kl} is the normalized strain field, and E_p is the normalized piezoelectric field. Therefore, the overall electrical–mechanical–optical (EMO) modulation has the following expression:

$$g_{EMO} = -\frac{\partial\omega}{\partial V_0}\Big|_{EMO} = \frac{g_{MO}g_{EM}}{\sqrt{(\Omega^2 - \Omega_b^2)^2 + \Gamma_m^2\Omega^2}}. \tag{5}$$

Considering both EMO and EO modulation, the cavity dynamics can be written as

$$\begin{aligned}\dot{a} &= -\frac{\kappa}{2}a - i(\omega_0 - g_{EMO}V_0\sin(\Omega t + \varphi_m) \\ &\quad - g_{EO}V_0\sin\Omega t)a + \sqrt{\kappa_{ex}}se^{-i\omega t}, \\ &= -\frac{\kappa}{2}a - i(\omega_0 - A\sin(\Omega t + \phi))a + \sqrt{\kappa_{ex}}se^{-i\omega t},\end{aligned} \tag{6}$$

under the existence of an exerted voltage between the electrodes $V = V_0\sin\Omega t$, where a is the annihilation operator of the optical mode, ω is the pump laser angular frequency, s is the optical pump, κ is the total loss rate, κ_{ex} is the external loss rate, and A and ϕ are the amplitude and phase response of combined EMO and EO effects.

As shown in Eq. (5), the EMO modulation has resonant behavior, while for the EO modulation, its amplitude and phase response should remain a constant while sweeping the microwave frequency, thus, resulting in a flat background in the S_{21} spectrum. By solving for the solution $a_p(t)$ of Eq. (6) and utilizing cavity input–output theory $|a_{out}|^2 = |-se^{-i\omega t} + \sqrt{\kappa_{ex}}a_p(t)|^2$, we could obtain the output optical signal oscillating at Ω. Under the resolved sideband limit $\Omega \gg \kappa$, and with a pump detuning $\Delta = \omega - \omega_0 \approx \pm\kappa/2$, the optical beating signal at Ω received by the photodetector (PD) in Fig. 2(a) is reduced to $|a_{out}|^2/|s|^2 \approx \mp\cos(\Omega t + \phi)\cdot(2\kappa_{ex}/\kappa)\cdot(A/\Omega)$. Since the

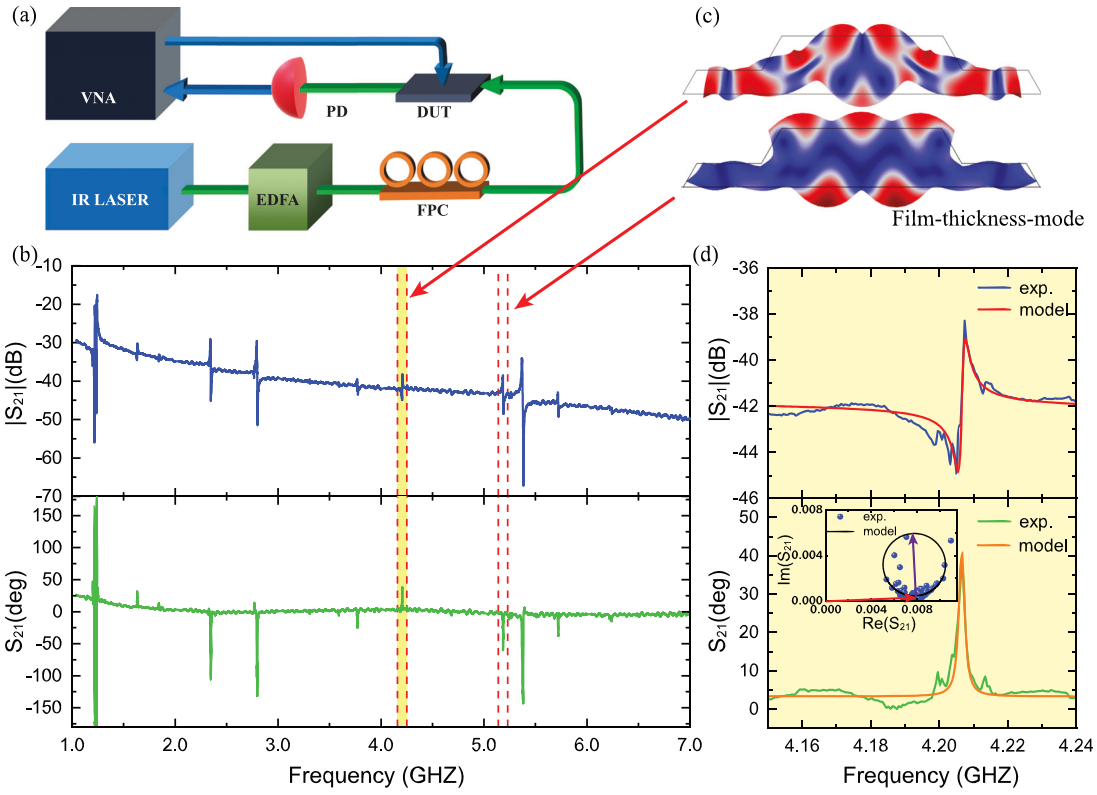

FIG. 2. (a) Measurement setup. (b) S_{21} spectrum when pumping at the slope of an optical resonance. (c) Simulation of mechanical eigenmodes. The bottom mechanical mode is the film thickness mode. (d) Zoom in of the 4.2 GHz resonance with a Q value of 2200, fitted using the model described above. The inset demonstrates the S_{21} phase diagram, with a red vector representing the EO modulation strength and a purple vector representing the EMO modulation strength.

electromechanical link is very under-coupled, the terminal impedance of the microwave transmission line does not change much when the frequency of the vector network analyzer (VNA) sweeps across the mechanical resonance. Therefore, the S_{21} signal measured by the setup depicted in Fig. 2(a) can be written as $|S_{21}| = k \cdot (2\kappa_{ex}/\kappa) \cdot (A/\Omega)$, $\angle S_{21} = \phi + \phi_0$, where k and ϕ_0 are assumed to be constants in the interested frequency range.

Figure 2(b) shows the measured S_{21} when the probe IR laser frequency is set at the slope of an optical resonance. The mechanical modes can be simulated using COMSOL Multiphysics, as seen in Fig. 2(c). One can find that the measured resonances are of Fano shape, resulting from the interference between EMO and EO modulation. Using the model we described above, we can extract the Q factor of the mechanical mode and the g_{EMO}/g_{EO} ratio by fitting the measured S_{21} response. An example of a 4.2 GHz mechanical resonance is shown in Fig. 2(d), with a fitted Q factor of 2200 and $|g_{EMO}/g_{EO}|_{\Omega=\Omega_b} = 0.7$ on the mechanical resonance. To understand the EMO and EO interference more intuitively, one can resort to the phase diagram shown in the inset of Fig. 2(d), where the resonant behavior of the mechanical mode shown in the phase diagram is circle like, while the non-resonant behavior of the EO modulation can be viewed as a vector that offsets the resonant circle. Here, the length of the red vector and purple vector in Fig. 2(d) represents the EO and EMO modulation strength, respectively. The ratio between the length of the purple vector and that of the red vector is the same as the absolute value of the ratio between g_{EMO} and g_{EO}, which is around 0.7 for this mechanical mode. From the COMSOL simulation, we obtain $|g_{MO}| = 2\pi \cdot 7.8 \times 10^6$ Hz/pm for the mechanical resonance around 4.2 GHz as shown in Fig. 2(d) and $|g_{EO}| = 2\pi \cdot 8.8 \times 10^7$ Hz/V (around 0.7 pm/V for the optical telecom band). The vacuum coupling rate defined by $g_{0,MO} = g_{MO}\sqrt{\hbar/2m_{eff}\Omega_b}$ gives an absolute value of $2\pi \cdot 288$ Hz, with an effective mass m_{eff} of 1.46 pg. Using the fitted ratio between g_{EMO} and g_{EO}, we further obtain $|g_{EM}| = 2.5 \times 10^6$ m/(V s^2), which relates the voltage and the maximum mechanical displacement. Thus, for a voltage of 1 V, the maximum displacement of such a mechanical mode is 7.83 pm. The corresponding microwave-to-phonon efficiency $\eta = \Gamma_e/\Gamma_m = \frac{\Gamma_m}{4} \cdot \frac{1}{2} m_{eff}\Omega_b^2\alpha^2 / \frac{(0.5V_0)^2}{2Z_0} = 3.8 \times 10^{-5}$, where Γ_e is the mechanical resonator coupling rate to the microwave channel, Γ_m is the total mechanical loss rate, V_0 is the voltage between the electrodes, and Z_0 is the characteristic impedance of the transmission line.

The mechanical mode of particular interest is the film thickness mode at 5.2 GHz as shown in Fig. 2(c). For the thickness mode, the simulated $|g_{MO}| = 2\pi \cdot 3.6 \times 10^7$ Hz/pm and $|g_{0,MO}| = 2\pi \cdot 1.7$ kHz, with an effective mass of 0.69 pg. To obtain the Q factor and microwave coupling efficiency of the thickness mode, fitting of the measured spectrum is required. However, around this thickness mode, there are several other mechanical modes that are only a few MHz away from the thickness mode as shown in Fig. 3 at 200 K. At room temperature, when the quality factor is not high enough, the optomechanical responses of those modes are similar in amplitude, and so the measured optomechanical response peak of the thickness mode is actually the envelope of mechanical modes around the thickness mode and the thickness mode cannot be resolved. To resolve the thickness mode, we perform measurements at cryogenic temperatures because the phonon loss is reduced at lower temperatures.[29]

The temperature dependence of the quality factor and frequency of thickness mode is shown in Fig. 3. As the temperature decreases

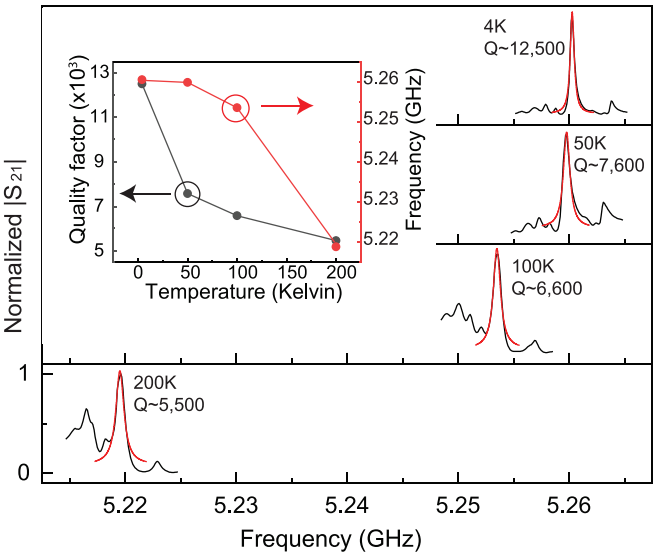

FIG. 3. Optomechanical response of the thickness mode at different temperatures from 4 to 200 K. The measurement setup is identical to that in Fig. 2, but with the device mounted in a cryostat. The temperature dependence of the quality factor and resonance frequency of the thickness mode is shown in the inset.

from 200 to 4 K, the quality factor of the thickness mode increases from 5500 to 12 500. With the increasing quality factor and, therefore, stronger resonance enhancement, the thickness mode has a stronger response as the temperature decreases. So the thickness mode stands out from the surrounding modes with decreasing temperature as shown in Fig. 3. At 4 K, an fQ product of 6.6×10^{13} is achieved, which approaches the state-of-the-art value of that on AlN platforms[30] and GaAs platforms[31] at similar temperatures. From the trend of the quality factor's dependence on temperature shown in the inset of Fig. 3, the fQ product could be higher at lower temperatures.

Resulting from the improved mechanical Q factor and, therefore, stronger microwave to mechanical coupling efficiency, the fitted $|g_{EMO}/g_{EO}|$ ratio at 4 K is approximately 13, with estimated $|g_{EM}| = 2.7 \times 10^6$ m/(V s^2) and $\eta = 1 \times 10^{-4}$. The microwave to phonon coupling efficiency could be further improved with the higher mechanical Q factor and by better impedance matching the microwave drive. A recent work on piezo-optomechanical transducer has demonstrated microwave to phonon coupling efficiency up to 17%.[18]

In summary, we demonstrate a high frequency piezo-optomechanical system up to 5.2 GHz by employing the film thickness mode on the thin film lithium niobate platform. The mechanical mode exhibits a high quality factor around 12 500 at 4 K, yielding a state-of-the-art fQ product on this important material platform. Together with a high optical quality factor, our system shows great potential for strong light modulation and efficient microwave-to-photon conversion.

AUTHORS' CONTRIBUTIONS

M.S. and J.X. contributed equally to this work.

This work was supported by ARO Grant No. W911NF-18–1-0020. H.X.T. acknowledges partial funding support from the NSF

EFRI grant (No. EFMA-1640959) and Packard foundation. Funding for substrate materials used in this research was provided by the DOE/BES grant under Award No. DE-SC0019406. The authors thank Yong Sun, Mike Rooks, Sean Rinehart, and Kelly Woods for their assistance provided in the device fabrication.

DATA AVAILABILITY

The data that support the findings of this study are available from the corresponding author upon reasonable request.

REFERENCES

[1]S. A. Tadesse and M. Li, "Sub-optical wavelength acoustic wave modulation of integrated photonic resonators at microwave frequencies," Nat. Commun. **5**, 5402 (2014).
[2]L. Fan, C.-L. Zou, M. Poot, R. Cheng, X. Guo, X. Han, and H. X. Tang, "Integrated optomechanical single-photon frequency shifter," Nat. Photonics **10**, 766–770 (2016).
[3]D. B. Sohn, S. Kim, and G. Bahl, "Time-reversal symmetry breaking with acoustic pumping of nanophotonic circuits," Nat. Photonics **12**, 91–97 (2018).
[4]L. Fan, C.-L. Zou, N. Zhu, and H. X. Tang, "Spectrotemporal shaping of itinerant photons via distributed nanomechanics," Nat. Photonics **13**, 323–327 (2019).
[5]A. H. Safavi-Naeini, D. Van Thourhout, R. Baets, and R. Van Laer, "Controlling phonons and photons at the wavelength scale: Integrated photonics meets integrated phononics," Optica **6**, 213 (2019).
[6]A. Vainsencher, K. J. Satzinger, G. A. Peairs, and A. N. Cleland, "Bi-directional conversion between microwave and optical frequencies in a piezoelectric optomechanical device," Appl. Phys. Lett. **109**, 033107 (2016).
[7]M. Forsch, R. Stockill, A. Wallucks, I. Marinković, C. Gärtner, R. A. Norte, F. van Otten, A. Fiore, K. Srinivasan, and S. Gröblacher, "Microwave-to-optics conversion using a mechanical oscillator in its quantum ground state," Nat. Phys. **16**, 69–74 (2020).
[8]W. Jiang, C. J. Sarabalis, Y. D. Dahmani, R. N. Patel, F. M. Mayor, T. P. McKenna, R. Van Laer, and A. H. Safavi-Naeini, "Efficient bidirectional piezo-optomechanical transduction between microwave and optical frequency," Nat. Commun. **11**, 1166 (2020).
[9]X. Han, W. Fu, C. Zhong, C.-L. Zou, Y. Xu, A. A. Sayem, M. Xu, S. Wang, R. Cheng, L. Jiang *et al.*, "10-GHz superconducting cavity piezo-optomechanics for microwave-optical photon conversion," arXiv:2001.09483 (2020).
[10]M. Mirhosseini, A. Sipahigil, M. Kalaee, and O. Painter, "Quantum transduction of optical photons from a superconducting qubit," arXiv:2004.04838 (2020).
[11]L. Fan, X. Sun, C. Xiong, C. Schuck, and H. X. Tang, "Aluminum nitride piezo-acousto-photonic crystal nanocavity with high quality factors," Appl. Phys. Lett. **102**, 153507 (2013).
[12]J. Bochmann, A. Vainsencher, D. D. Awschalom, and A. N. Cleland, "Nanomechanical coupling between microwave and optical photons," Nat. Phys. **9**, 712–716 (2013).
[13]W. Fu, Z. Shen, Y. Xu, C.-L. Zou, R. Cheng, X. Han, and H. X. Tang, "Phononic integrated circuitry and spin–orbit interaction of phonons," Nat. Commun. **10**, 2743 (2019).
[14]L. Ding, C. Baker, P. Senellart, A. Lemaitre, S. Ducci, G. Leo, and I. Favero, "Wavelength-sized GaAs optomechanical resonators with gigahertz frequency," Appl. Phys. Lett. **98**, 113108 (2011).
[15]K. C. Balram, M. I. Davanço, J. D. Song, and K. Srinivasan, "Coherent coupling between radiofrequency, optical and acoustic waves in piezo-optomechanical circuits," Nat. Photonics **10**, 346–352 (2016).
[16]R. S. Weis and T. K. Gaylord, "Lithium niobate: Summary of physical properties and crystal structure," Appl. Phys. A **37**, 191–203 (1985).
[17]M. Zhang, C. Wang, R. Cheng, A. Shams-Ansari, and M. Lončar, "Monolithic ultra-high-Q lithium niobate microring resonator," Optica **4**, 1536 (2017).
[18]L. Shao, M. Yu, S. Maity, N. Sinclair, L. Zheng, C. Chia, A. Shams-Ansari, C. Wang, M. Zhang, K. Lai, and M. Lončar, "Microwave-to-optical conversion using lithium niobate thin-film acoustic resonators," Optica **6**, 1498 (2019).
[19]W. Jiang, R. N. Patel, F. M. Mayor, T. P. McKenna, P. Arrangoiz-Arriola, C. J. Sarabalis, J. D. Witmer, R. Van Laer, and A. H. Safavi-Naeini, "Lithium niobate piezo-optomechanical crystals," Optica **6**, 845 (2019).
[20]S. G. Hofer, W. Wieczorek, M. Aspelmeyer, and K. Hammerer, "Quantum entanglement and teleportation in pulsed cavity optomechanics," Phys. Rev. A **84**, 052327 (2011).
[21]D. E. Chang, K.-K. Ni, O. Painter, and H. J. Kimble, "Ultrahigh-Q mechanical oscillators through optical trapping," New J. Phys. **14**, 045002 (2012).
[22]R. A. Norte, J. P. Moura, and S. Gröblacher, "Mechanical resonators for quantum optomechanics experiments at room temperature," Phys. Rev. Lett. **116**, 147202 (2016).
[23]T. P. McKenna, J. D. Witmer, R. N. Patel, W. Jiang, R. Van Laer, P. Arrangoiz-Arriola, E. A. Wollack, J. F. Herrmann, and A. H. Safavi-Naeini, "Cryogenic microwave-to-optical conversion using a triply-resonant lithium niobate on sapphire transducer," arXiv:2005.00897 (2020).
[24]Y. Chu, P. Kharel, W. H. Renninger, L. D. Burkhart, L. Frunzio, P. T. Rakich, and R. J. Schoelkopf, "Quantum acoustics with superconducting qubits," Science **358**, 199–202 (2017).
[25]X. Han, K. Y. Fong, and H. X. Tang, "A 10-GHz film-thickness-mode cavity optomechanical resonator," Appl. Phys. Lett. **106**, 161108 (2015).
[26]Y. Yang, R. Lu, T. Manzaneque, and S. Gong, "1.7 GHz Y-cut lithium niobate mems resonators with FoM of 336 and fQ of 9.15×10^{12}," in 2018 IEEE/MTT-S International Microwave Symposium-IMS (2018), pp. 563–566.
[27]R. Wang, S. A. Bhave, and K. Bhattacharjee, "Design and fabrication of S_0 lamb-wave thin-film lithium niobate micromechanical resonators," J. Microelectromech. Syst. **24**, 300–308 (2015).
[28]S. G. Johnson, M. Ibanescu, M. A. Skorobogatiy, O. Weisberg, J. D. Joannopoulos, and Y. Fink, "Perturbation theory for maxwell's equations with shifting material boundaries," Phys. Rev. E **65**, 066611 (2002).
[29]E. Spencer and P. Lenzo, "Temperature dependence of microwave elastic losses in $LiNbO_3$ and $LiTaO_3$," J. Appl. Phys. **38**, 423–424 (1967).
[30]X. Han, W. Fu, C. Zhong, C.-L. Zou, Y. Xu, A. Al Sayem, M. Xu, S. Wang, R. Cheng, L. Jiang *et al.*, "Cavity piezo-mechanics for superconducting-nanophotonic quantum interface," arXiv:2001.09483v2 (2020).
[31]D. T. Nguyen, C. Baker, W. Hease, S. Sejil, P. Senellart, A. Lemaître, S. Ducci, G. Leo, and I. Favero, "Ultrahigh q-frequency product for optomechanical disk resonators with a mechanical shield," Appl. Phys. Lett. **103**, 241112 (2013).